SHOCK DEFORMATION IN ZIRCON, A COMPARISON OF RESULTS FROM SHOCK-REVERBERATION AND SINGLE-SHOCK EXPERIMENTS. T. M. Erickon[1,2,3], C. J. Cline[1,2], R. Jakubek[1,2], M. J. Cintala[2] and N. E. Timms[3], [1]Jacobs-JETS contract, 2224 Bay Area Boulevard, Houston, TX, 77058, USA (Timmons.m.erickson@nasa.gov), [2]Astromaterials Research and Exploration Science division, NASA JSC, XI3, 2101 NASA Parkway, Houston, TX, 77058, USA, [3]Space Science and Technology Center, School of Earth and Planetary Science, GPO Box 1984, Perth, WA, 6845, Australia.

Introduction: The utility of the mineral zircon, $ZrSiO_4$, as a shock-metamorphic geobarometer and geochronometer, has been steadily growing within the planetary science community. Zircon is an accessory phase found in many terrestrial rock types (e.g., [1]), lunar samples (e.g., [2]), lunar meteorites (e.g., [3]), martian meteorites (e.g., [4]) and various other achondrites (e.g., [5]). Because zircon is refractory and has a high closure temperature for Pb diffusion [6], it has been used to determine the ages of some of the oldest material on Earth [7] and elsewhere in the Solar System [5]. Furthermore, major (O) and trace-element (REE, Ti, Hf) abundances and isotope compositions of zircon help characterize the petrogenetic environments and sources from which they crystallized.

The response of zircon to impact-induced shock deformation is predominantly crystallographic, including dislocation creep and the formation of planar and sub-planar, low-angle grain boundaries; the formation of mechanical {112} twins [8, 9]; transformation to the high pressure polymorph reidite [10, 11]; the development of polycrystalline microtextures [12]; and dissociation to the oxide constituents SiO_2 and ZrO_2 [13]. Shock microstructures can also variably affect the U-Pb isotope systematics of zircon [14, 15] and, in some instances, be used to constrain the impact age.

While numerous studies have characterized shock deformation in zircon recovered from a variety of terrestrial impact craters and ejecta deposits (e.g., [14, 15, 16]) and Apollo samples [8, 17], experimental studies of shock deformation in zircon are limited to a handful of examples in the literature (e.g., [17, 18]). In addition, the formation conditions (e.g., P, T) of various shock microstructures, such as planar-deformation bands, twins, and reidite lamellae, remain poorly constrained. Furthermore, previous shocked-zircon experimental charges have not been analyzed using modern analytical equipment. This study will therefore undertake an new set of zircon shock experiments, which will then be microstructurally characterized using state-of-the-art instrumentation within the Astromaterials Research and Exploration Science Division (ARES), NASA Johnson Space Center.

Experimental Methods: We have performed a series of shock-deformation experiments on natural zircon megacrysts from the Mudtank Carbonatite, Northern Territory, Australia [20]. Two experiments were performed using the flat-plate accelerator (FPA), four experiments were undertaken using the vertical gun (VG), and one experiment with a two stage light-gas gun (LGG), housed in the Experimental Impact Lab within ARES. The shock-reverberation experiments using the FPA were undertaken with large, oriented zircon crystals, cut normal to [001] and [hkl]. The fragments were surrounded by randomly oriented zircon powder within a tungsten-alloy sample container and shocked to pressures of 21.2 and 18.2 GPa, respectively. The single-shock VG experiments included a single-crystal oriented normal to [001] and bimodal zircon powders which were fired into copper targets at speeds of 1.1, 1.2, 1.6 and 2.6 km/s. One-dimensional shock-stress calculations using the hugoniots for copper and zircon yielded stresses of 19.5, 21.3, 28.4, and 41.8 GPa, respectively. The LGG single-shock experiment used a lexan slug with a zircon epoxied to the tip; it was launched at 4.7 km/s into a copper target, achieving a peak pressure 106 GPa.

Analytical methods: Zircon fragments were extracted from the FPA sample container and from craters within the VG and LGG targets. The fragments were mounted in epoxy and polished for analysis with fine sub-50 nm colloidal silica. The shocked-zircon charges were then imaged using the JEOL 7600F field emission gun scanning electron microscope housed in the E-Beam suite of ARES. Deformation microstructures and high pressure polymorphs were characterized with electron backscatter diffraction (EBSD) maps collected using an Oxford Instruments Symmetry detector with a 20 kV accelerating voltage, 15 nA beam current, 17.5 mm working distance and 500 – 100 µm step size. Laser Raman microscopy provided additional confirmation of high pressure phases and shock using a WITec alpha300R confocal microscope.

Results: The 18.2 GPa FPA zircon experiment displays a cleavage of four irregularly spaced sets of (sub-) planar fractures in reflected light and backscattered electron (BSE) images. Microstructural EBSD mapping reveals large (>9°) crystal-plastic strain concentrated in planar deformation bands that run parallel to the developed cleavage within the grain, consistent with slip in both <100>[010] and <001>[100] (Fig. 1 A). Laser Raman mapping of the sample shows that the

$\nu_3(SiO_4)$ stretching band at 1006 cm^{-1} has an average full width of 8-10.5 cm^{-1} with fractures having larger bandwidths. Reidite, the high pressure polymorph of zircon, was not detected in either the EBSD or laser Raman maps.

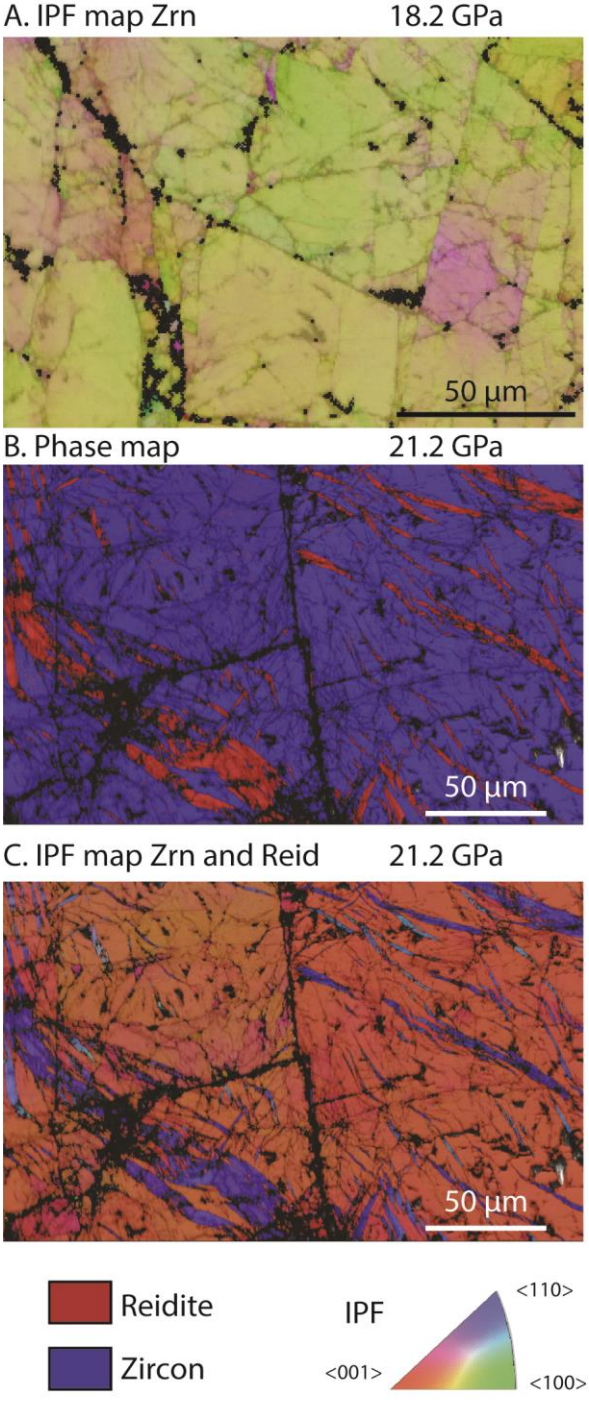

Figure 1. Electron backscatter diffraction maps of experimental shocked zircon. A. Inverse pole figure (IPF) map of zircon shocked to 18.2 GPa. B and C. Phase and IPF maps of zircon with reidite lamellae shocked to 21.2 GPa.

The 21.2 GPa [001] oriented FPA experiment also displays a cleavage in reflected light and BSE images; however, the cleavage is cross-cut by distinctive sets of lamellae. Crystallographic EBSD maps reveal that the cross-cutting lamellae are composed of reidite (Fig. 1 B & C). Internally, the reidite is twinned with systematic misorientations of 70° about <110>, which are consistent with a habit plane (K_1) of {112} and a shear direction (η_1) of <111>, similar to [19]. The zircon crystal lattice is highly strained and displays up to 8° of misorientation resulting from cumulative strain and discrete planar deformation bands. Raman imaging shows 1006 cm^{-1} bandwidths are comparable to the 18.2 GPa shocked sample but Raman spectra consistent with reidite are also observed.

Conclusions: The shocked zircon experiments presented herein establish new pressure constraints on the formation conditions of shock microstructures in zircon. Previous experiments by [19] produced reidite at 40 GPa but not at 20 GPa, while our study shows that reidite forms at 21.2 GPa under reverberation conditions. All analyzed experiments show the development of a cleavage within zircon and the formation of planar deformation bands, while {112} mechanical twins have not been identified. Future work will characterize (EBSD and laser Raman) the single-shock charges at 19.5, 21.3, 28.4, 41.8 and 106 GPa and compare the resulting microstructures with those from the shock-reverberation experiments presented herein and by [19].

References: [1] Hoskin P. W. O. & Schaltegger U. (2003) *Rev. in Min. and Geochem., 53,* 27–62. [2] Nemchin A. A. et al. (2009) *Nat. Geo. ,2,* 133–136. [3] Demidova S. I. et al. (2014) *Petrology,* 22, 1–16. [4] Humayun M. et al. (2013) *Nature, 503,* 513–516. [5] Ireland T. R. & Wlotzka F. (1992) *EPSL, 109,* 1–10. [6] Cherniak D. J. & Watson E. B. (2003) *Rev. in Min. and Geochem., 53,* 113–143. [7] Wilde S. A. et al. (2001) *Nature, 409,* 175–178. [8] Timms N. E. et al. (2012) *MAPS, 47,* 120–141. [9] Erickson T. M. et al. (2013) *Am. Min., 98,* 53–65. [10] Glass B. P. & Liu S. (2001) *Geology, 29,* 371 – 373. [11] Erickson T. M. et al. (2017) *Con. Min. Pet., 172*. [12] Cavosie A. J. et al. (2016) *Geology, 44,* 703–706. [13] Timms N. E. et al. (2017) *EPSL, 477,* 52–58. [14] Moser D. E. et al. (2011) *Can. J. Earth Sci., 48,* 117–139. [15] Schmieder M. et al. (2015) *GCA, 161,* 71 – 100. [16] Singleton A. C. et al. (2015) *GSA Special Publication 518,* 135–148. [17] Crow C. A. et al. (2018) *MAPS, 54,* 181 – 201. [18] Mashimo T. et al. (1983) *Physics and Chemistry of Minerals, 9* , 237 – 247. [19] Leroux H. et al. (1999) *EPSL, 169,* 291 – 301. [20] Black L. P. & Gulson B. L. (1978) *Journal of Aus. Geo. and Geophys. 3,* 277 – 232.